N87-28790

# DSS 63 64-Meter Antenna S- and X-Band Efficiency and System Noise Temperature Calibrations, July 1986

S. D. Slobin

Radio Frequency and Microwave Subsystems Section

*The DSN 64-m antenna in Spain (DSS 63) has been calibrated prior to its upgrading to a 70-m High Efficiency configuration in preparation for the Voyager Neptune encounter in August 1989. The S-band (2285-MHz) and X-band (8420-MHz) effective area efficiency and system noise temperature calibrations were carried out during July 1986 to establish a baseline system performance for this station. It is expected that the 70-m upgrade will result in at least a 1.9-dB G/T improvement at X-band relative to the 64-meter baseline reference. This article is the first in a series which will document 64-m and High Efficiency 70-m and 34-m antenna performance improvements due to size increase, high-precision surface panel installation, dual-shaped reflector profiles for uniform illumination, microwave holographic surface panel adjustment, or combinations of the above elements.*

## I. Introduction

The DSN 64-m antenna network (DSS 14, 43, 63) is being upgraded in preparation for the Voyager Neptune encounter, and also to enable acceptable performance at frequencies higher than X-band. In particular, the antenna diameter is being increased to 70 meters, the main reflector and subreflector profiles are being shaped (in contrast to standard paraboloidal and hyperboloidal forms), high-precision shaped main reflector panels are being installed, and an extensive series of focusing and panel setting operations are being undertaken. The measurements reported here were made at the S- and X-band frequencies of 2285 MHz and 8420 MHz, respectively.

The existing 34-m High Efficiency antennas (DSS 15, 45, 65), which already have shaped reflector surfaces, will have their panels set using microwave holographic techniques recently developed at JPL and elsewhere.

This article is the first in a series which will document the performance of the 64/70-m antennas in the pre-70-m (1986/87) and post-70-m (1987/88) configurations, as well as the performance of the 34-m High Efficiency antennas. At the present time, calibration efforts will concentrate on the High Efficiency antennas; however, the older 34-m Ha-Dec antennas will be re-calibrated at the conclusion of the present efforts. The results of these calibrations will be used to update DSN/Flight Project Interface Design documents and telecommunication prediction and performance analysis computer programs.

The antenna calibration technique was performed using a computer-based method commonly referred to as the MDA/NAR technique. The Metric Data Assembly Noise Adding Radiometer (MDA/NAR) is used to measure system noise temperatures when the antenna is alternately pointed at a calibra-

tion radio source and then at a nearby cold-sky location. The entire gain and noise temperature calibration methodology is embodied in three software packages: RADIOMETRY, MDA/NAR, and AGA/9600. RADIOMETRY generates source location predictions that drive the antenna during the radio source observation. MDA/NAR generates on- and off-source noise temperature estimates during a radio source observation period. AGA/9600 determines antenna pointing corrections, corrections for source size, and estimates of antenna efficiency at each particular observation point. The entire antenna gain calibration procedure is described elsewhere.[1]

A major factor during the July 1986 DSS 63 64-m calibration was the choice of the Madrid station-developed MDA/NAR methodology over the JPL-developed BP-80 NAR technique, a similar noise-adding radiometer antenna calibration method. Both techniques were extensively evaluated in parallel use. This choice has effectively cemented the MDA/NAR technique into the DSN antenna calibration program for the duration of the antenna testing period for the next several years. What was desired was an accurate radiometric system, capable of quasi-automatic data acquisition (gain and pointing) at any DSN complex. The MDA/NAR proved slightly more accurate due to the method of handling typical small receiver nonlinearities. The BP-80 NAR, an earlier development, included a method for handling small detector nonlinearities, but not receiver nonlinearities. Hence, the MDA/NAR technique resulted in improved overall accuracy. Also, the MDA/NAR provided the desired quasi-automatic data acquisition, whereas the BP-80 did not. On the other hand, the MDA/NAR, while fulfilling the dedicated application for which it was designed, falls short in related applications where the BP-80 proves versatile and occasionally necessary. For example, initial antenna RF alignment tasks (lateral and axial focusing, and sidelobe-level checks) are conveniently accomplished using the BP-80 manual and real-time data reduction necessary to proceed with on-site measurements. The MDA/NAR, requiring a separate data reduction process (using the same computer previously utilized for data acquisition), proves cumbersome and time consuming for any real-time decision-dependent work cycle. Error analysis of the MDA/NAR is discussed in Section IV of this article.

A typical MDA/NAR-supported observation process is as follows: A natural radio source is chosen for at least several hours of observation. The antenna moves to an off-source position near the radio source (typically 0.240 degree) so that the measured system noise temperature represents the contribution of ground and atmosphere only (in addition to

the constant hardware contribution). For a period of about 4 minutes, the radio source is scanned in the azimuth and elevation directions. From measurements of noise temperature and antenna position, the antenna efficiency and pointing error can be determined, with suitable small corrections made for source size and pointing error.

The radio-source calibrators used at DSS 63 (and their S/X-band flux densities, Janskys) were 3C274 (140.00/46.00), 3C123 (32.00/10.15), 3C286 (11.78/5.435), 3C218 (27.7/8.34), and 3C161 (13.05/4.075). These sources are considered to exhibit stable flux levels with time and are therefore suitable for use as standard gain calibrators. The DSN has adopted standard radio source flux densities for the calibration sources. (A description of previous efficiency measurements at 8420 MHz and the radio sources used is given in [1].) For a 100-percent area-efficient antenna, the expected increase in system noise temperature from a natural radio source is given by

$$\Delta T_s = S A_p / 2 k$$

where

$S$ = flux density of the radio source, W/m²-Hz

$A_p$ = physical area of the antenna, m²

$k$ = Boltzmann's constant (1.380622E-23), W/Hz-K

The actual gain of the antenna (for 100-percent area efficiency) is given by

$$G(\text{ratio}) = 4\pi A_p / \lambda^2$$

where

$A_p$ = physical area of antenna

$\lambda$ = wavelength

For a 64-m-diameter antenna, at 8420 MHz (X-band), the 100-percent efficient gain is 75.04 dBi. At 2285 MHz (S-band), the 100-percent efficient gain is 63.71 dBi.

To the extent the 100-percent area-efficient system noise temperature increase is not achieved, the measured area efficiency of the antenna may thus be determined. Included in the measured area efficiency is the attenuating effect of the atmosphere, resulting in an estimate of efficiency that is too low. This can be accounted for by atmospheric modeling or by actual measurements of atmospheric parameters at the time of the calibration.

---

[1]*Antenna Gain Calibration Procedure, 70-Meter Upgrade Project*, JPL Document Number D-3794 (internal document), Jet Propulsion Laboratory, Pasadena, Calif., November 15, 1986.

Efficiency and noise temperature curves are presented both with and without atmospheric effects included. It is recommended that for all telecommunications link analyses, the "atmosphere-free" antenna parameters be used. In this way the *total* real or postulated atmospheric attenuation and noise temperature can be included in the analysis. (Existing design documents present antenna gain and system noise temperature *including* atmospheric effects—a confusing situation.)

## II. Antenna Area Efficiency

Figures 1 and 2 show the measured S-band antenna efficiencies both with and without the atmospheric attenuation effect, respectively. The S-band atmospheric model is based on the accepted [2] zenith attenuation of 0.03 dB, corresponding to a standard clear atmosphere. At 30-degree elevation angle (2 airmasses in the flat-earth approximation) the attenuation is doubled to 0.06 dB. (An attenuation loss of 0.03 dB corresponds to an effective loss of efficiency of 0.688 percent for a perfect antenna.) For antennas with less than 100-percent efficiency, this loss of efficiency is not entirely experienced. The actual area efficiency without atmospheric attenuation is determined by

$$\text{efficiency (w/o atm)} = \text{efficiency (w/atm)} \times L$$

where

$$L = 10^{A(dB)/10}, \geqslant 1$$

$A(dB)$ = attenuation at elevation angle of interest

Therefore, because of the inherent nonperfect antenna efficiency, the entire effect of atmospheric removal is not realized. In other words, the removed atmospheric attenuation is not simply added to the antenna efficiency. In the manner described above, the measured antenna efficiencies with atmospheric loss were modified at each elevation angle to calculate the inherent antenna efficiency as though no atmosphere were present. By using the no-atmosphere efficiency curves, without the confusing compensations for included atmospheric loss, the effects of varying atmospheric conditions (large at higher frequencies) can be accounted for more readily in later determinations of overall telecommunications link performance.

Second-order curves were fitted to the data shown in Figs. 1 and 2. These curves are of the form

$$\text{efficiency} = a_0 + a_1\theta + a_2\theta^2$$

where

$\theta$ = elevation angle, degrees

The coefficients of this expression for the S-band efficiency curves are given in Table 1.

In a similar manner, the X-band efficiency curves were calculated both with and without the standard clear-atmosphere attenuation effects. For X-band, the atmospheric model uses an accepted [2] zenith attenuation of 0.04 dB, which corresponds to a total signal loss of 0.917 percent for a perfect antenna. Figures 3 and 4 show the X-band efficiencies both with and without atmospheric effects included. The coefficients of the efficiency curve-fits are also given in Table 1. Included in Table 1 are the peak values of efficiency, the elevation at which these peak values occur, and the standard deviation of the curve fit.

It should be appreciated that the simple atmospheric modeling used at S- and X-bands is quite appropriate. Heavy cloud cover and/or rain precludes calibration measurements. For future work at higher frequencies (e.g., Ka-band) it is envisioned that the technique of measuring off-source system noise temperature as a function of elevation angle will be used to obtain better estimates of the atmospheric loss during specific measurement sessions.

It is seen that in the X-band efficiency curves, the efficiency falls off rather rapidly at angles away from the peak angle. DSS 63 is unique in that structural braces were added with the goal of reducing antenna gain change due to main reflector distortion. However, original bracing which was to have been removed to provide the final configuration was intentionally retained for an interim period due to scheduling problems. Since the DSS 63 subreflector *y-z* focusing movement was developed for a slightly differently configured antenna, it is felt that the gain fall-off results from incorrect subreflector movement in attempting to compensate for main reflector distortion and quadripod sag. The DSS 63 results at both S- and X-band should be considered atypical. Indeed, measurements on the other 64-m antennas do not show this large change of efficiency with elevation angle. (The subreflector *y-z* focusing curves which were operational during the measurements reported here are defined elsewhere.[2])

## III. System Noise Temperature

Part of the antenna efficiency determination is a measurement of off-source system noise temperature. Figures 5 and 6 show raw data determinations of S- and X-band system noise temperatures as a function of elevation angle for several radio

---

[2]JPL Software Specification Document No. DFA-5222-OP, *Antenna Mechanical Subsystem—Subreflector Controller for 64 m Antennas* (internal document), Jet Propulsion Laboratory, Pasadena, Calif., March 21, 1986.

sources on two different days. For X-band, the "prime" and "backup" maser preamplifier curves include different waveguide noise temperature contributions due partially to different path lengths in the receiving system. The 12-inch-longer path length of the prime maser contributes approximately 1 K, and the prime maser has approximately 1-K higher noise temperature. This accounts for the 2-K difference between system noise temperatures for the two systems. The prime X-band maser is designated as X-TWM1 (S/N 2006). The backup X-band maser is X-TWM2 (S/N 2003). Both are Block II masers. The S-band maser is designated S-TWM1 (S/N 4001).

Figure 7 shows solid-curve approximations to the experimental data. These curves are not extrapolated below a 10-degree elevation angle, the lower limit of the experimental data. Because of the large number of airmasses below 10-degree elevation (greater than 6 airmasses), care should be taken in obtaining noise temperature estimates in the 0- to 10-degree elevation region. The horizontal inhomogeneity of the atmosphere makes extrapolation in elevation a source of significant error in noise temperature modeling.

As with the efficiency determinations, the atmospheric noise temperature effects can be removed from the raw data by suitable atmospheric models. At S-band, the 0.03-dB zenith attenuation corresponds to a noise temperature contribution of 1.93 K; the 0.04-dB X-band zenith attenuation corresponds to 2.57-K noise temperature. These models assume an effective atmospheric physical temperature of 280 K. The noise temperature contribution that is removed is determined from

$$T_{atm} = 280 \times \left(1 - \frac{1}{L}\right)$$

where $L$ = atmospheric loss factor (described earlier). Figure 8 shows the three noise temperature curves with the atmospheric noise, as modeled, removed. Table 2 indicates the fourth-order curve fit coefficients and standard deviations of curve fit for the curves shown in Figs. 7 and 8. Both sets of X-band backup maser data have been combined into one curve.

## IV. Error Analysis

Despite extensive and continuing error analysis of both the BP-80 and MDA/NAR radiometers from July 1986 through the present, a full accuracy statement is not yet possible. It must be remembered that all raw measured values are of system noise temperature, and thus depend on the initial calibration of the noise diode, the noise diode stability, receiver linearity, and a knowledge of maser noise contribution—a value which may have changed slightly since initial construc-

tion and testing. These are the major sources of instrumental systematic errors.

As a matter of perspective, however, it is unlikely that instrumental systematic errors exceeding ±0.2 dB (±5 percent) with $3\sigma$ confidence are present. Random errors in the determination of antenna efficiency (cf. Figs. 1 and 3) are estimated to be ±0.15 dB at S-band, and ±0.2 dB at X-band ($3\sigma$). The largest source of inaccuracy in the measurement of X-band antenna system efficiency remains the basic radio astronomical flux density absolute accuracy, which is estimated to be ±0.5 dB ($3\sigma$) (±4%, $1\sigma$ [1]). At S-band, it is estimated that there exists a flux density accuracy of somewhat less than ±0.3 dB with similar $3\sigma$ confidence [3]. Assuming these estimated error sources to be independent, it is seen that the radio source flux density is the largest contributor to uncertainty in the rms estimate of antenna efficiency. The absolute accuracy in the determination of antenna efficiency for the DSS 63 antenna can thus be stated as:

S-band: ±0.4 dB ($3\sigma$)

X-band: ±0.6 dB ($3\sigma$)

Continued refinement of noise temperature measurement techniques will not significantly alter these values, as the present limiting factor in efficiency determination is the knowledge of radio source flux density.

As radio source flux density is not a factor in system noise temperature determination, this large error source may be neglected in this analysis. Random errors in the determination of off-source noise temperature may be somewhat less than those seen in antenna efficiency, as the noise temperature is a raw data measurement and not subject to random pointing errors and corrections. It is estimated that for both S- and X-band, the random noise temperature determination errors are less than 0.1 dB ($3\sigma$). Thus the remaining uncertainties, systematic and random, yield the following estimates of noise temperature tolerances:

S/X-band: ±0.22 dB ($3\sigma$)

The corresponding uncertainties at a nominal 25-K system noise temperature are:

S/X-band: ±1.5 K ($3\sigma$)

The two main sources of error in the data analysis phase (as opposed to experimental errors in data gathering) are curve fitting and atmospheric correction.

Standard deviations of curve fits are stated in Tables 1 and 2 for the efficiency and noise temperature curves. These values are essentially the random errors quoted earlier. For the

efficiency curves, the standard deviations are less than 1 efficiency-percent. For noise temperatures, the standard deviations are better than 0.25 K for the curves shown in Fig. 8. Extrapolations for noise temperature below about a 10-degree elevation angle (the lowest experimental point) should be made with care.

The source of clear-sky atmospheric models is [2]. As the atmospheric conditions during the calibration measurements are not known beyond the fact that there existed a clear sky, some amount of atmospheric modeling error exists. It is estimated, based on experience, that zenith atmospheric model errors of less than 20 percent ($1\sigma$) exist, which would result in efficiency errors not exceeding 0.1 percent ($1\sigma$) at zenith for a 50-percent efficient antenna.

A comprehensive error analysis covering the entire antenna calibration process, including important systematic error estimation and radiometer accuracy analysis, will be published in a later *TDA Progress Report*.[3]

## V. Comparison of Measured and Expected Antenna Efficiencies

In this section, the elements contributing to the net X-band area efficiency of the DSS 63 64-m antenna are given and discussed. A comparison with measured efficiencies is made using models developed from physical optics (PO) analysis and geometrical theory of diffraction (GTD) analysis, modified by other losses as described below. As the theoretical models do not include an atmospheric effect, the comparison is made with the X-band no-atmosphere best-fit curve shown in Fig. 4.

The existing PO analysis program[4] does not consider the effect of main reflector distortion and subreflector focusing as a function of elevation angle. It does, however, allow a detailed analysis of feed system parameters affecting overall antenna efficiency. The gain/efficiency effects of large-scale (tens of meters, laterally) ordered distortions of the main reflector are calculated using the GTD program[5] using the surface specified by structural analysis. The effects of small-scale distortions (centimeters to meters, laterally) due to main and subreflector surface roughness and panel manufacturing and

---

[3] R. Riggs, Jet Propulsion Laboratory, private communication, May 1987.

[4] A. Cha, *Physical Optics Analysis of NASA/JPL Deep Space Network 70-m Antennas*, JPL D-1853 (internal document), Jet Propulsion Laboratory, Pasadena, Calif., November 1984.

[5] T. Veruttipong, D. Rochblatt, W. Imbriale, and V. Galindo, *Dual Shaped and Conic GTD/Jacobi-Bessel Analysis Programs, A User Manual*, JPL D-2583 (internal document), Jet Propulsion Laboratory, Pasadena, Calif., July 30, 1985.

setting tolerance are given by the so-called Ruze loss [4]. This Ruze loss can be applied to results of both the PO and GTD programs. Thus both programs are capable of describing antenna performance at 45-degree elevation (or whatever rigging angle results in a "perfect" antenna shape); however, only the GTD program yields efficiency determinations over the entire range of elevation angles.

The physical optics program assumes perfect antenna shape and subreflector position, and hence is equivalent to calculations made for an actual antenna at an elevation angle of 45 degrees where the main reflector is designed and set to have a perfect paraboloidal shape. The feed system analyzed here uses a dual hybrid mode horn. Table 3 lists the expected feed system losses. In addition, hardware losses are given, including those arising from reflector panel manufacturing and setting tolerances. The subreflector and panel tolerances total 1.06 mm, rms. It is seen that feed system losses (items 2 through 7) reduce the 100-percent area efficiency by 1.02 dB, to a net effective antenna gain of 74.02 dBi. This value is compared with the equivalent GTD-calculated gain of 74.13 dBi. For the purposes of this article, these gain values are deemed to be identical, and both methods are regarded as equivalently predicting antenna performance. Further losses (a total of 0.82 dB) show the effect of the non-feed components such as waveguide loss, dichroic plate loss, VSWR, quadripod blockage, and the Ruze loss components described above. An rms surface tolerance of 1.06 mm results in a Ruze loss of 0.61 dB.

The efficiency value of 0.569 has not been achieved at 45-degree elevation by any 64-m antenna in the DSN, although the Goldstone antenna, DSS 14, has achieved 52 percent, 0.39 dB below the 56.9-percent expectation given by the PO program. DSS 14 64-m efficiency measurements will be made in late 1987 and will be reported in a later *TDA Progress Report*.

Figure 9 shows a comparison of measured antenna area efficiency (without atmosphere, Fig. 4) and expected values of efficiency as given by GTD calculations of antenna gain, reduced by known or postulated hardware losses. The PO-equivalent losses (Table 3, items 2–7) are not determined separately by GTD, but are accounted for internally. Additional loss (a total of 0.821 dB) from waveguide (0.070 dB), dichroic plate (0.035 dB), VSWR (0.039 dB), and quadripod blockage (0.677 dB) reduces the GTD-calculated antenna gain. Also, an efficiency loss due to small-scale surface roughness is considered, and the level of roughness expected is that given in Table 3 (i.e., 1.06 mm, rms). The net efficiency factor due to this loss is given by the Ruze formula

$$\eta = \exp\left[-\left(\frac{4\pi\epsilon}{\lambda}\right)^2\right]$$

where

$\epsilon$ = small-scale surface roughness

$\lambda$ = wavelength

It is seen that although the shapes of the two curves are similar, there exists a substantial difference between expected and measured curves. The measured efficiency for DSS 63 is 1.12-dB lower than the expected efficiency. Figure 10 shows similar curves which will help explain these results. The five curves shown include the Fig. 9 curves, plus three additional curves of GTD-calculated efficiency for Ruze surface roughness of 1.5, 1.8, and 2.0 mm, rms. The measured (Fig. 4) data shown in Figs. 9 and 10, when compared with the GTD-calculated efficiency curves, give quite good performance agreement if one accepts a 1.7- to 1.8-mm rms level of small-scale surface roughness, which is certainly reasonable for a well-used and aged 64-m antenna. The K-band (11.45-GHz) holography measurements with 0.4-m resolution made in May 1985 with the extra antenna brace installed, indicate an rms surface error, measured normal to the best-fit paraboloid, of 1.53 mm at a 40-degree elevation angle. This rms surface error includes the Ruze loss plus a small gravity-induced distortion. This is entirely consistent with the 1.7- to 1.8-mm Ruze tolerance described above. It was predicted[6] that panel adjustment would reduce the rms surface error to 0.86 mm. Thus, it is seen that this type of analysis confirms the use of GTD to predict antenna performance, and also puts upper limits on the tolerances of the assumed and/or measured values of the losses described earlier.

In summary, it is seen that PO and GTD programs agree within about 0.1 dB at the point the computations can be compared with one another. At that point, a reasonable assumption of small-scale surface roughness virtually identically matches the experimental data defining antenna efficiency vs. elevation angle.

We consider the DSS 63 64-m July 1986 S/X-band calibrations to be very successful. As discussed, absolute area efficiency accuracies are clearly limited by radio source flux accuracies, and when flux and instrumental systematic errors are combined with random measurement errors, we obtain area efficiency error estimates of $\pm0.4$ dB ($3\sigma$ confidence) at S-band and $\pm0.6$ dB ($3\sigma$) at X-band. Absolute noise temperature accuracies, an equally important parameter in SNR-limited telecommunication links, are found to be $\pm0.22$ dB ($3\sigma$) at both bands. This translates, for a nominal 25-K system, to $\pm1.5$-K ($3\sigma$) accuracy.

---

[6] M. P. Godwin, et al., "Final Report on Holographic Tests at S-band and K-band on the DSS-63 64 Metre Antenna", Report No. A087, Job No. 50/042, Eikontech Limited, Sheffield, England, February 1986.

# Acknowledgment

# References

[1] J. A. Turegano and M. J. Klein, "Calibration radio sources for radio astronomy: Precision flux density measurements at 8420 MHz," *Astronomy and Astrophysics*, vol. 86, pp. 46–49, 1980.

[2] E. K. Smith, "Centimeter and millimeter wave attenuation and brightness temperature due to atmospheric oxygen and water vapor," *Radio Science*, vol. 17, No. 6, pp. 1455–1464, November–December 1982.

[3] A. J. Freiley, P. D. Batelaan, and D. A. Bathker, "Absolute flux density calibrations of radio sources: 2.3 GHz," *JPL Technical Memorandum 33-806*, Jet Propulsion Laboratory, Pasadena, Calif., December 1, 1977.

[4] J. Ruze, "Antenna tolerance theory—A review," *Proceedings of the IEEE*, vol. 54, No. 4, pp. 633–640, April, 1966.

**Table 1. Coefficients of second-order curve fits for antenna area efficiencies**

$$\text{efficiency} = a_0 + a_1\theta + a_2\theta^2$$

where $\theta$ = elevation angle, degrees

| Coefficient/Parameter | S-Band (2285 MHz) | X-Band (8420 MHz) |
|---|---|---|
| | With Atmosphere (cf. Fig. 1) | With Atmosphere (cf. Fig. 3) |
| $a_0$ | 54.25744 | 32.69687 |
| $a_1$ | 8.635463E-02 | 0.4869833 |
| $a_2$ | −6.788819E-04 | −4.959421E-03 |
| Peak efficiency, % | 57.004 | 44.652 |
| Peak angle, deg | 63.601 | 49.097 |
| Standard deviation, % | 0.676 | 0.767 |
| | Without Atmosphere (cf. Fig. 2) | Without Atmosphere (cf. Fig. 4) |
| $a_0$ | 56.30269 | 34.80555 |
| $a_1$ | 3.554052E-02 | 0.4332722 |
| $a_2$ | −2.862227E-04 | −4.540844E-03 |
| Peak efficiency, % | 57.406 | 45.141 |
| Peak angle, deg | 62.085 | 47.708 |
| Standard deviation, % | 0.679 | 0.822 |

**Table 2. Coefficients of fourth-order curve fits for S- and X-band system noise temperatures**

$$T_{system} = a_0 + a_1\theta + a_2\theta^2 + a_3\theta^3 + a_4\theta^4$$

where $\theta$ = elevation angle, degrees

| Coefficient/Parameter | S-Band (2285 MHz)[a] | X-Band (8420 MHz)[b], Prime Maser | X-Band (8420 MHz)[c], Backup Maser |
|---|---|---|---|
| | With Atmosphere (cf. Fig. 7) | With Atmosphere (cf. Fig. 7) | With Atmosphere (cf. Fig. 7) |
| $a_0$ | 5.652297E+01 | 6.267107E+01 | 6.146491E+01 |
| $a_1$ | −1.618135E+00 | −2.483746E+00 | −2.613738E+00 |
| $a_2$ | 3.732890E−02 | 6.249823E−02 | 6.721768E−02 |
| $a_3$ | −3.992906E−04 | −7.002778E−04 | −7.637453E−04 |
| $a_4$ | 1.607969E−06 | 2.884866E−06 | 3.171873E−06 |
| Zenith noise temperature, K | 27.671 | 24.143 | 22.028 |
| Standard deviation, K | 0.198 | 0.390 | 0.389 |
| | Without Atmosphere (cf. Fig. 8) | Without Atmosphere (cf. Fig. 8) | Without Atmosphere (cf. Fig. 8) |
| $a_0$ | 3.670053E+01 | 3.638264E+01 | 3.507050E+01 |
| $a_1$ | −4.414013E−01 | −9.301171E−01 | −1.046979E+00 |
| $a_2$ | 6.952927E−03 | 2.255099E−02 | 2.677656E−02 |
| $a_3$ | −5.212648E−05 | −2.452661E−04 | −3.015780E−04 |
| $a_4$ | 1.566596E−07 | 9.880078E−07 | 1.239911E−06 |
| | | Note: If $\theta \geqslant 80°$, $T_{system}$ = 21.192 K | Note: If $\theta \geqslant 85°$, $T_{system}$ = 19.056 K |
| Zenith noise temperature, K | 25.571 | 21.192 | 19.056 |
| Standard deviation, K | 0.071 | 0.231 | 0.135 |

[a]S-band (2285 MHz) specifications: maser S-TWM1; S/N 4001; and 2.5 K noise temperature.
[b]X-band (8420 MHz) specifications: prime maser; X-TWM1; S/N 2006; and 3.7 K noise temperature.
[c]X-band (8420 MHz) specifications: backup maser; X-TWM2; S/N 2003; and 2.03 K noise temperature.

**Table 3. Design expectations for 64-m antenna with dual hybrid mode feedhorn at 8420 MHz and 45-degree elevation angle using physical optics analysis**

| Item | Loss, dB | Net Gain, dBi |
|------|----------|---------------|
| 1. 100% Area Efficiency | | 75.04 |
| 2. Illumination Amplitude | −0.454 | |
| 3. Illumination Phase | −0.146 | |
| 4. Forward and Rear Spillover | −0.210 | |
| 5. Subreflector Blockage | −0.170 | |
| 6. $m \neq 1$ modes | −0.035 | |
| 7. Cross polarization | −0.0004 | 74.02 |
| 8. Waveguide loss | −0.070 | |
| 9. Dichroic plate loss | −0.035 | |
| 10. VSWR | −0.039 | |
| 11. Quadripod Blockage | −0.677 | |
| 12. Main reflector panels | | |
|     Manufacturing (0.035 inches) | −0.430 | |
|     Setting (0.019 inches) | −0.127 | |
| 13. Subreflector | | |
|     Manufacturing (0.012 inches) | −0.051 | 72.59 (= 0.569 efficiency) |

Note: The rms panel and subreflector tolerance = 0.04159 in. (1.06 mm)
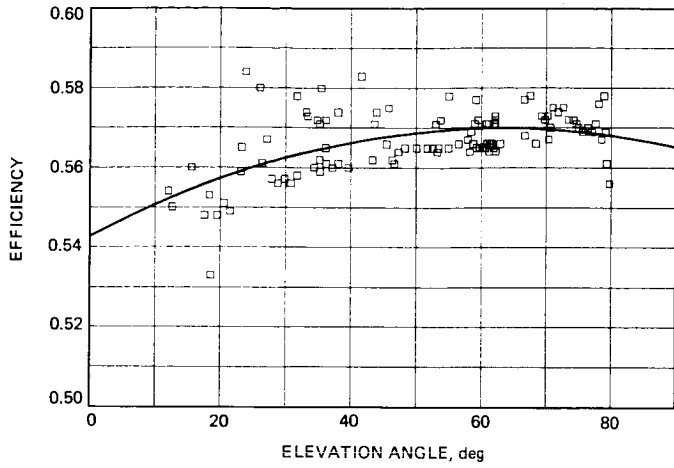
Fig. 1. DSS 63 64-m S-band (2285-MHz) area efficiency with atmospheric attenuation included
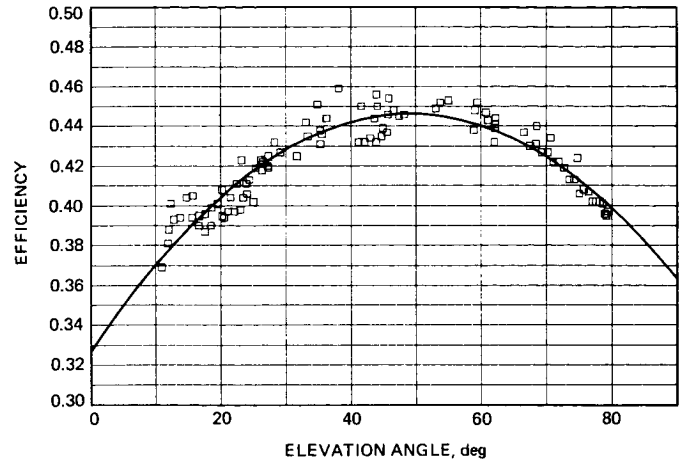


Fig. 3. DSS 63 64-m X-band (8420-MHz) area efficiency with atmospheric attenuation included
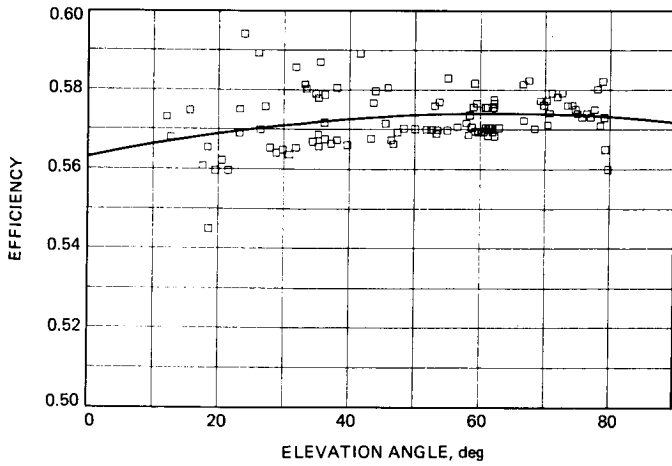


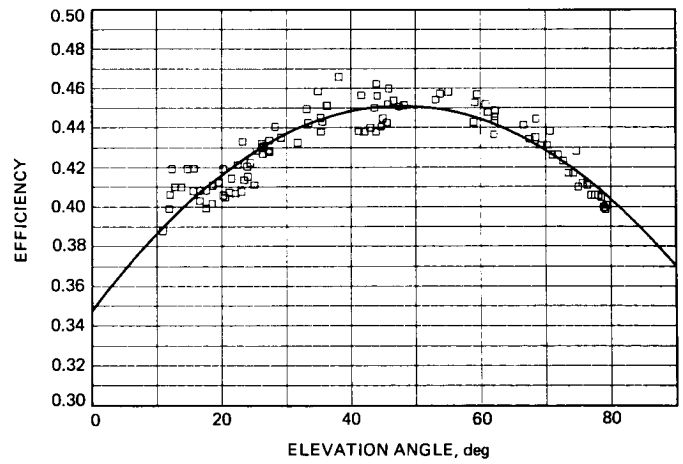Fig. 2. DSS 63 64-m S-band (2285-MHz) area efficiency without atmospheric attenuation



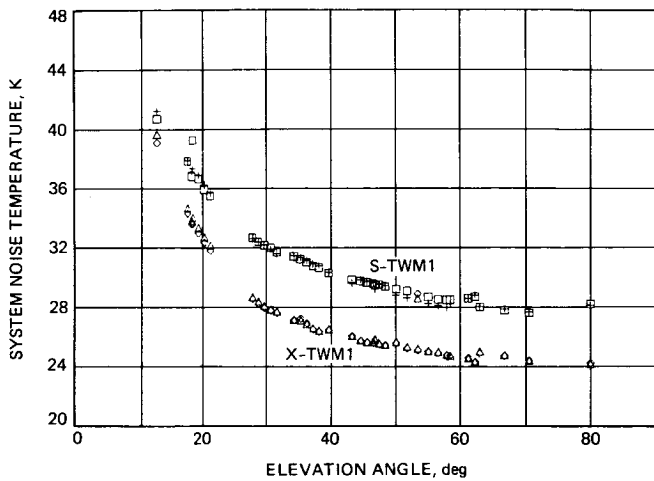Fig. 4. DSS 63 64-m X-band (8420-MHz) area efficiency without atmospheric attenuation

**Fig. 5. DSS 63 64-m system noise temperature raw data, S-band (2285-MHz) and X-band (8420-MHz) prime maser, including atmospheric contribution**
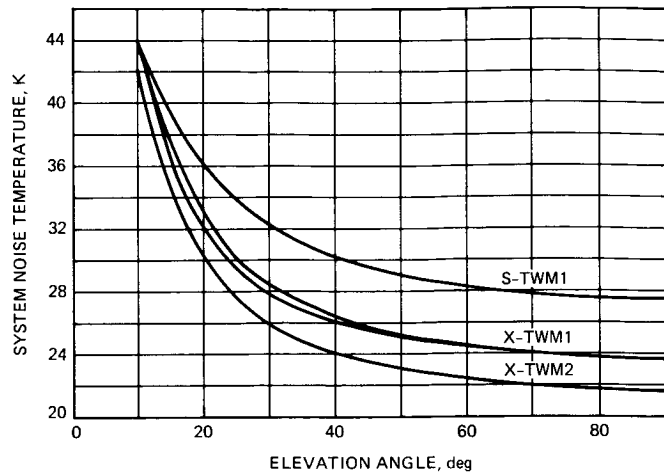


**Fig. 7. DSS 63 64-m system noise temperature solid-curve approximations to raw data, S-band (2285 MHz) and X-band (8420 MHz), including atmospheric contribution**
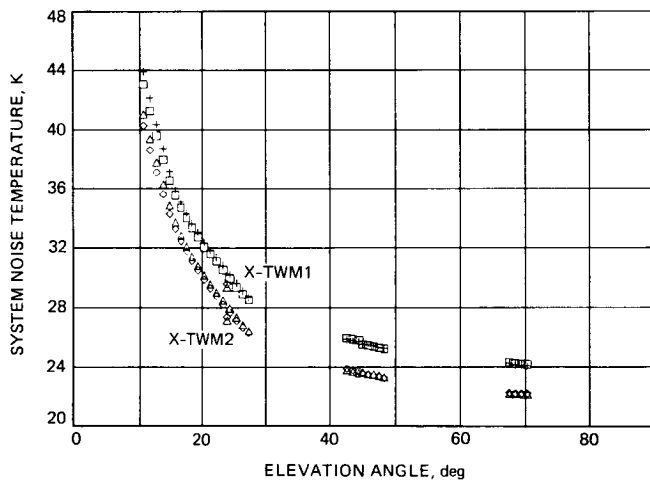


**Fig. 6. DSS 63 64-m system noise temperature raw data, X-band (8420-MHz) prime maser and X-band backup maser, including atmospheric contribution**
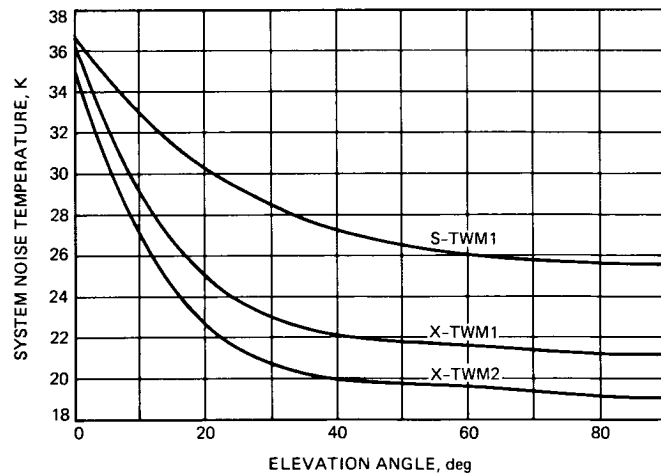


**Fig. 8. DSS 63 system noise temperture models, S-band (2285 MHz) and X-band (8420 MHz), without atmospheric contribution**
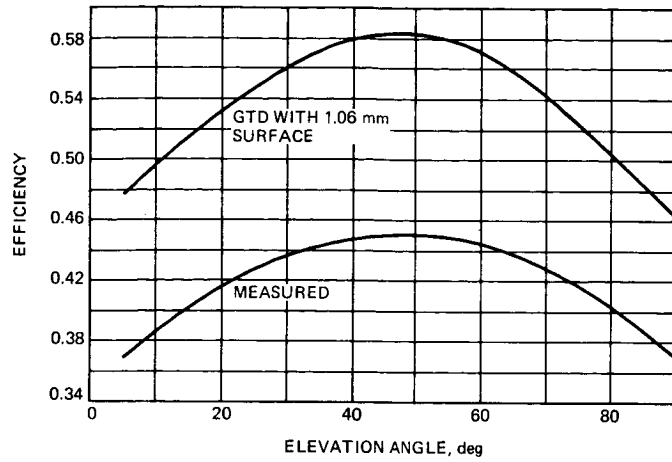
**Fig. 9. Comparison of DSS 63 64-m GTD-calculated efficiency (with 1.06-mm-rms Ruze surface tolerance) and measured efficiency**
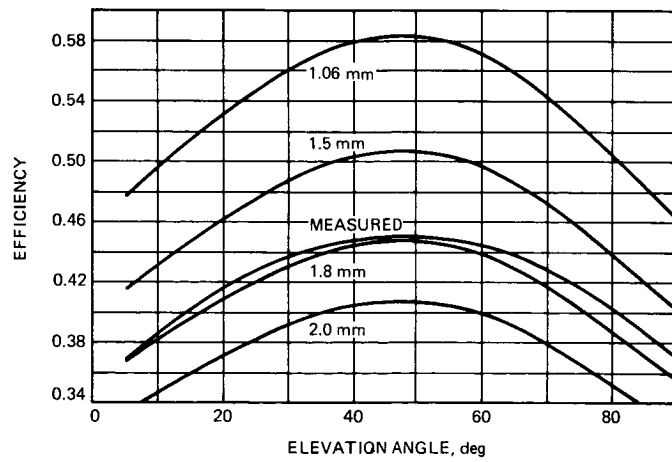


**Fig. 10. Comparison of DSS 63 64-m GTD-calculated efficiency and measured efficiency for various Ruze surface tolerance values**